SAND2013-1853C

Simulating the Response of External Stores on Aircraft Using Linear and Nonlinear Vibroacoustics

Michael R. Ross*, Timothy Walsh†, Jerry W. Rouse‡,
D. Gregory Tipton§, Eric Stasiunas¶,
Sandia National Laboratories, Albuquerque, NM, 87106, USA

Mathew Lawry‖,
University of Colorado, Boulder, CO, USA

James Freymiller**
ATA Engineering, San Diego, CA, USA

One of the more severe environments for stores carried on high performance military aircraft is the external captive carry environment. This paper presents methods for simulating this environment using linear and nonlinear vibroacoustics. The store is modeled using linear finite elements, but the acoustics are modeled with linear or nonlinear finite elements depending on the level of acoustic excitation. Guidelines for when to use nonlinear acoustic elements are provided. The method is first compared to a diffuse acoustic field and then to actual flights.

I. Introduction

As a greater emphasis on computational analysis develops, component level predicted responses are being requested from full system analysis. Due to space limitations, several components cannot be instrumented to provide the input level to the specific component for a given environment. An environment that can drive component design and specification for weapon stores is the captive carry environment.

There are two primary methods for modeling the captive carry environment. The first method uses a computational fluid dynamics (CFD) code coupled to a computational structural dynamics (CSD) code.[1,2] This is computationally intensive, and is being reserved for internal captive carry (inside a bomb bay), where the flow field is complex, highly nonlinear, and unsteady. It is possible to capture the unsteady pressure loading beneath a turbulent boundary layer of a free store using statistical models which account for the magnitude, temporal, and spatial correlation of large coherent structures within the boundary layer. At realistic flight conditions, an unsteady turbulent boundary layer is too computationally expensive to simulate directly, and instead, empirical and theory-based models are developed to represent the unsteady wall pressure under the boundary layer. Sandia National Laboratories is making progress in this effort.[3] These models have been created and tested for reentry vehicles. Currently, work is underway to verify and validate this work for weapon stores at Sandia National Laboratories.

The second method for modeling the captive carry environment is done with the use of vibroacoustics. When the flow field is not complex and generally steady, the aerodynamic turbulence loading can also be modeled using an acoustic profile. It has been shown that external captive carry can be well represented with vibroacoustics.[4] In addition, a vibroacoustic simulation is more computationally efficient and aligns better with proposed environmental ground tests.

In the vibroacoustic simulation, the vibration portion represents the air frame structural motions caused by the aerodynamics of the aircraft and the engine vibration. The acoustic spectrum, defined in terms of

*Senior Member R&D Staff, Analytical Structural Dynamics Dept., MS-0346, mross@sandia.gov, Senior Member AIAA.
†Senior Member R&D Staff, Computational Solid Mechanics and Structural Dynamics Dept., MS-0380, tfwalsh@sandia.gov
‡Senior Member R&D Staff, Analytical Structural Dynamics Dept., MS-0346, jwrouse@sandia.gov
§Principal Member R&D Staff, Analytical Structural Dynamics Dept., MS-0346, dgtipto@sandia.gov
¶Senior Member R&D Staff, Experimental Environment Simulation Dept., MS-0557, ecstasi@sandia.gov
‖Graduate Student, University of Colorado, Aerospace Engineering Dept., mwlawry@sandia.gov
**ATA Engineering, james.freymiller@ata-engineering.com

Sound Pressure Level (SPL), predominantly represents the turbulent boundary layer pressure fluctuations caused by the flow field around the store. A CFD code can be used to provide the acoustic profile.

This work presents a method for simulating the vibroacoustic environment using an in-house finite element (FE) code, SIERRA SD.[5] Significant work has been done using both FE and statistical energy analysis (SEA) for representing acoustics.[6,7] The finite element representation was chosen due to the ability in SIERRA SD to model nonlinear acoustics.[8] This work shows that the levels of the external captive carry environment require nonlinear acoustics to obtain the correct environment.

Before the full vibroacoustic predictions of external captive carry are performed, model calibration is required. The calibration is accomplished by comparing a diffuse acoustic field (DAF) experiment in a reverberant chamber to simulated results. Unfortunately, the SPL attainable, 130 dB OASPL (Overall Sound Pressure Level), in the reverberant chamber is 35 dB below the environment specifications for the system of interest.

The calibrated model can be used to make predictions for actual flight conditions. The results are compared to true flight tests. The comparison is accomplished knowing that the root mean square acceleration response (GRMS) is proportional to the dynamic pressure for flight conditions where the dominant source of excitation is turbulent boundary layer flow.[9,10] Results are presented that are within the variability of flight tests. This validates the method of vibroacoustic simulations proposed in this work.

This paper is organized as follows. Section II describes the differences between the linear acoustic implementation and the nonlinear acoustic implementation in the CSD code, SIERRA SD. Section III provides theoretical limits for when it is appropriate to use linear and nonlinear acoustics. This is followed by comparing simulations to an acoustic experiment in Section IV. It is believed that portions of the frequency content behave nonlinearly in this experiment. Section V gets to the crux of the matter with comparisons of simulations to actual flight test data. Conclusions and summary are provided in Section VI.

II. Finite Element Representation of Linear and Nonlinear Acoustics

This section presents the derivation of the weak formulations of the linear and nonlinear equations of motion. Eventually, it is shown that the additional terms in the nonlinear weak formulation affect the system by driving energy from lower frequencies to higher frequencies. The nonlinear effects increase the frequency of the sound waves. In addition, the nonlinear formulation can handle waves with finite amplitude.

There are several issues with the implementation of acoustic-structure interaction: non-matching meshes, the boundary conditions on the wetted interface, how the different physics are coupled, non-reflecting boundary conditions, acoustic scattering, etc.; however, the focus in this work is on the differences between linear and nonlinear acoustics. This is needed to help explain the observed differences between the simulated acoustics and the acoustic experiment described in Section IV. Interested readers can be referred to the SIERRA SD theory manual for details of implementation of acoustic-structure interaction.[5]

The linear formulation of acoustics begins with linear acoustic wave equation,

$$\frac{1}{c^2}\frac{\partial^2\psi}{\partial t^2} - \Delta\psi = 0, \tag{1}$$

where ψ is the velocity potential ($\dot{u} = \nabla\psi$, $\dot{u}$ is the particle velocity), Δ represents the Laplacian of the scalar ψ ($\nabla^2\psi = \Delta\psi$), and c is the speed of sound. A weak formulation of equation 1 can be constructed by multiplying with a test function and integrating by parts. Denote the fluid domain by Ω_f and its boundary by $\partial\Omega = \partial\Omega_n \bigcup \partial\Omega_d$, where the subscripts n and d refer to the portions of the boundary where Neumann and Dirichlet boundary conditions are applied. It is assumed that the fluid is initially at rest, i.e. $\psi(x,0) = \dot{\psi}(x,0) = 0$, which is sufficient for most applications.

Denoting by $V_f(\Omega_f)$ the function space for the fluid, the weak formulation can be written as follows. Find the mapping $\psi: \quad [0,T] \rightarrow V_f(\Omega_f)$ such that

$$\frac{1}{c^2}\int_\Omega \ddot{\psi}\phi d\Omega + \int_\Omega \nabla\psi\cdot\nabla\phi d\Omega = -\int_{\partial\Omega_n} \rho_f \dot{u}_n \phi d\Omega_n \tag{2}$$

$\forall\phi \in V_f(\Omega_f)$, where $\dot{u}_n$ is the prescribed normal velocity on the Neumann portion of the fluid boundary. Inserting a finite element discretization $\psi(x) = \sum_{i=1}^{N}\psi_i N_i(x)$ into Eq. 2 results in the system of equations

$$M\ddot{\psi} + K\psi = f_a, \tag{3}$$

where N is the vector of shape functions, $M = \int_{\Omega_f} \frac{1}{c^2} N^T N d\Omega_f$ is the mass matrix, $K = \int_{\Omega_f} \nabla N^T \cdot \nabla N d\Omega_f$ is the stiffness matrix, and $f_a = \int_{\partial\Omega_n} \rho_f \dot{u}_n N^T d\Omega_n$ is the external forcing vector from Neumann boundary conditions.

Linear acoustic theory is based on the assumptions of small amplitude waves and a linear constitutive theory of the fluid medium. Although these assumptions hold for many vibroacoustic interactions, they are invalid in sound fields with high sound pressure levels,[11,12,13] i.e. sound fields that have *finite amplitude waves*. The classical Kuznetsov equation[14] treats three-dimensional nonlinear acoustic waves to second order in nonlinearity. SIERRA SD uses a finite element implementation of the Kuznetsov wave equation. An abbreviated derivation of the system of equations for nonlinear acoustic is given next to help illustrate the differences.

The derivation begins with a nonlinear isentropic equation of state for air

$$\frac{P}{P_0} = \left(\frac{\rho}{\rho_0}\right)^{\gamma}, \tag{4}$$

where P and P_0 are the total and reference pressures, ρ and ρ_0 are the current and reference densities, and γ is the ratio of specific heats that is equal to 1.4 for air. Equation 4 can then be combined with the conservation of momentum and conservation of mass for the fluid to derive nonlinear wave equations. The equation of state, Eq. 4, is first expanded in a Taylor series about the isentrope $s = s_0$[11]

$$p = P - P_0 = \left(\frac{\partial P}{\partial \rho}\right)_{s_0,\rho_0} (\rho - \rho_0) + \frac{1}{2}\left(\frac{\partial^2 P}{\partial \rho^2}\right)_{s_0,\rho_0} (\rho - \rho_0)^2 + ..., \tag{5}$$

which can be written compactly as

$$p = A\left(\frac{\rho - \rho_0}{\rho_0}\right) + \frac{B}{2}\left(\frac{\rho - \rho_0}{\rho_0}\right)^2 + ..., \tag{6}$$

where $A = \rho_0 \left(\frac{\partial P}{\partial \rho}\right)_{s_0,\rho_0} \equiv \rho_0 c_0^2$, and $B = \rho_0^2 \left(\frac{\partial^2 P}{\partial \rho^2}\right)_{s_0,\rho_0}$. Since $\left(\frac{\partial P}{\partial \rho}\right)_{s_0,\rho_0} = c_0^2$ is simply the square of the linear speed of sound, it is noted from the expansion that the ratio of the first two terms is

$$\frac{B}{A} = \frac{\rho_0}{c_0^2}\left(\frac{\partial^2 P}{\partial \rho^2}\right)_{s_0,\rho_0}. \tag{7}$$

The parameter B/A accounts for the nonlinear constitutive law of the fluid up to second order. A table of values of B/A for various fluids can be found in texts on nonlinear acoustics.[11]

For linear acoustics, only the first term in the expansion 6 is retained. In that case,

$$p = A\left(\frac{\rho - \rho_0}{\rho_0}\right) = c_0^2(\rho - \rho_0), \tag{8}$$

which implies that the stiffness of the fluid is simply the square of the linear speed of sound.

Kuznetsov's equation uses the above Taylor series expansion of the equation of state, but truncates all terms past the second. It also accounts for convective nonlinearities to second order. The equation is derived by combining the Taylor series expansion of the equation of state with the conservation of mass and momentum. The result is the following:[14,13]

$$\frac{1}{c^2}\frac{\partial^2 \psi}{\partial t^2} - \Delta\psi - \frac{1}{c^2}\frac{\partial}{\partial t}\left(b(\Delta\psi) + \frac{B/A}{2c^2}\left(\frac{\partial \psi}{\partial t}\right)^2 + (\nabla\psi)^2\right) = 0. \tag{9}$$

The first two terms in equation 9 are the same as in equation 1, but the fourth and fifth terms are nonlinear. The third term is actually a linear absorption term, but it is usually grouped with the nonlinear terms to indicate deviation from the linear wave equation. The parameter b is for absorption in the fluid due to viscosity and thermal conductivity.

In a similar manner to Eq. 2, a weak formulation can be constructed. However, a minor modification is made. For a simpler output methodology, it is preferred to solve for ψ such that $p = \dot{\psi}$. This simply

involves a re-scaling in terms of density in equation 9. The weak formulation is now found by mapping $\psi: \quad [0,T] \rightarrow V_f(\Omega_f)$ such that

$$\frac{1}{c^2}\int_\Omega \ddot{\psi}\phi dx + \int_\Omega \nabla\psi\cdot\nabla\phi dx$$
$$+\frac{1}{c^2}\int_\Omega b\nabla\dot{\psi}\cdot\nabla\phi dx - \frac{1}{\rho c^4}(B/A)\int_\Omega \ddot{\psi}\dot{\psi}\phi dx -$$
$$\frac{2}{\rho c^2}\int_\Omega \nabla\dot{\psi}\cdot\nabla\psi\phi dx = \int_{\partial\Omega_n}\frac{\partial\psi}{\partial n}\phi ds = -\int_{\partial\Omega_n}\rho_f(\dot{u}_n + \frac{b}{c^2}\ddot{u}_n)\phi ds \tag{10}$$

$\forall\phi \in V_f(\Omega_f)$, where $\dot{u}_n$, and $\ddot{u}_n$ are the prescribed normal particle velocity and acceleration on the Neumann portion of the fluid boundary. It is noted that for air, $\frac{b}{c^2}$ is of the order $1e^{-10}$ under normal conditions, and thus it is usually sufficient to drop the acceleration term and approximate the right hand side as $-\int_{\partial\Omega_n}\rho_f\dot{u}_n\phi ds$.

A finite element formulation of equation 10 is constructed by representing the unknown by a finite summation $\psi(x) = \sum_{i=1}^n \psi_i N_i(x) = \psi^T N$, and substituting in equation 10. This leads to the following set of nonlinear ordinary differential equations in time.

$$F_{int}(\ddot{\psi}(x,t), \dot{\psi}(x,t), \psi(x,t)) = F_{ext}(x,t), \tag{11}$$

where

$$F^{int} = \frac{1}{c^2}\int_\Omega \ddot{\psi}\phi d\Omega + \int_\Omega \nabla\psi\cdot\nabla\phi d\Omega \tag{12}$$
$$+\frac{1}{c^2}\int_\Omega b\nabla\dot{\psi}\cdot\nabla\phi d\Omega - \frac{1}{\rho c^4}(B/A)\int_\Omega \ddot{\psi}\dot{\psi}\phi d\Omega -$$
$$\frac{2}{\rho c^2}\int_\Omega \nabla\dot{\psi}\cdot\nabla\psi\phi d\Omega, \tag{13}$$

and

$$F_{ext} = -\int_{\partial\Omega_n}\rho_f\dot{u}_n\phi d\Omega_n. \tag{14}$$

F^{int} is the internal force, which depends on ψ and its first two time derivatives, and F^{ext} is the external force. It is noted that $\ddot{\psi}$ and $\dot{\psi}$ actually depend on ψ through the time discretization scheme, and equation 11 could be written as

$$F_{int}(\psi(x,t)) = F_{ext}(x,t). \tag{15}$$

In order to linearize equation 11, we could use a finite difference approach, in which the tangent matrix is derived by differencing the internal force function with respect to an incremental displacement. Alternatively, we could derive a full Newton tangent matrix by taking partial derivatives with respect to all of the independent variables. In this work we have chosen to use the initial Newton method, where only the initial symmetric tangent needs to be formed, and the nonlinear terms are all accounted for on the right hand side residual term. The numerical experiments conducted thus far indicate that acceptable convergence behavior is observed with the initial Newton method.

We define $\tilde{\psi}, \tilde{\dot{\psi}}, \tilde{\ddot{\psi}}$ as the current iterates, and $\psi, \dot{\psi}, \ddot{\psi}$ as the unknowns. The tangent equations can be derived by expanding the left hand side of equation 11 in a Taylor series. If we truncate all terms beyond the constant and linear contributions, we obtain

$$F_{int}(\psi,\dot{\psi},\ddot{\psi}) \approx F_{int}(\tilde{\psi},\tilde{\dot{\psi}},\tilde{\ddot{\psi}}) +$$
$$\left[\frac{\partial F_{int}}{\partial\psi}(\tilde{\psi},\tilde{\dot{\psi}},\tilde{\ddot{\psi}}) + \frac{\partial F_{int}}{\partial\dot{\psi}}(\tilde{\psi},\tilde{\dot{\psi}},\tilde{\ddot{\psi}})\frac{\partial\dot{\psi}}{\partial\psi} + \frac{\partial F_{int}}{\partial\ddot{\psi}}(\tilde{\psi},\tilde{\dot{\psi}},\tilde{\ddot{\psi}})\frac{\partial\ddot{\psi}}{\partial\psi}\right]\Delta\psi = F_{int}(\tilde{\psi},\tilde{\dot{\psi}},\tilde{\ddot{\psi}}) + A\Delta\psi, \tag{16}$$

where $\Delta\psi = \psi - \tilde{\psi}$, and $\tilde{\psi}$ is the current iterate. The full tangent matrix A is defined as

$$A = \left[\frac{\partial F_{int}}{\partial\psi}(\tilde{\psi},\tilde{\dot{\psi}},\tilde{\ddot{\psi}}) + \frac{\partial F_{int}}{\partial\dot{\psi}}(\tilde{\psi},\tilde{\dot{\psi}},\tilde{\ddot{\psi}})\frac{\partial\dot{\psi}}{\partial\psi} + \frac{\partial F_{int}}{\partial\ddot{\psi}}(\tilde{\psi},\tilde{\dot{\psi}},\tilde{\ddot{\psi}})\frac{\partial\ddot{\psi}}{\partial\psi}\right]. \tag{17}$$

Since $\Delta\psi$ is unknown, we approximate it as $\Delta\tilde{\psi} = \tilde{\psi} - \tilde{\tilde{\psi}}$, where $\tilde{\tilde{\psi}}$ is the previous iterate. Thus, as convergence occurs, the current and previous iterates become identical.

We have chosen the generalized alpha time integration scheme in order to discretize equation 11 in time. The generalized alpha method is based on the generalized Newmark method. The flexibility of this method is useful in this case, since it can be made to be either implicit or explicit (e.g. central difference), depending on the problem at hand. In displacement form, the generalized Newmark method first needs an update equation. Given $\Delta\tilde{\psi}$, and a previous iterate $\tilde{\tilde{\psi}}$, we compute an updated current iterate as

$$\tilde{\psi} = \tilde{\tilde{\psi}} + \Delta\tilde{\psi}. \tag{18}$$

Then, we use $\tilde{\psi}$ to compute updated first and second time derivatives as follows

$$\begin{aligned}
\tilde{\tilde{\dot{\psi}}} &= \frac{1}{\beta\Delta t^2}\left[\tilde{\psi} - \psi_n - \dot{\psi}_n\Delta t\right] - \frac{1-2\beta}{2\beta}\ddot{\psi}_n, \\
\tilde{\dot{\psi}} &= \dot{\psi}_n + \Delta t\left[(1-\gamma)\ddot{\psi}_n + \gamma\tilde{\tilde{\dot{\psi}}}\right] \\
&= \dot{\psi}_n + \Delta t\left[(1-\gamma)\ddot{\psi}_n + \frac{\gamma}{\beta\Delta t^2}\left[\tilde{\psi} - \psi_n - \dot{\psi}_n\Delta t\right] - \gamma\frac{1-2\beta}{2\beta}\ddot{\psi}_n\right],
\end{aligned} \tag{19}$$

where γ, β are the integration parameters for the Newmark method, and $\dot{\psi}_n$, $\ddot{\psi}_n$ are the first and second time derivatives from the previous time step. Note that, as $\Delta\tilde{\psi} \to 0$, $\tilde{\psi} \to \psi_{n+1}$, indicating that the current iterate has converged to the value at the next time step, step $n+1$.

We can simplify by noting that, from equation 19,

$$\begin{aligned}
\frac{\partial\dot{\psi}}{\partial\psi} &= \frac{\gamma}{\beta\Delta t}, \\
\frac{\partial\ddot{\psi}}{\partial\psi} &= \frac{1}{\beta\Delta t^2}.
\end{aligned} \tag{20}$$

We also make the following definitions, which define the tangent stiffness, damping, and mass matrices

$$\begin{aligned}
\frac{\partial F_{int}}{\partial\psi}(\tilde{\psi}, \tilde{\dot{\psi}}, \tilde{\ddot{\psi}}) &= K_t, \\
\frac{\partial F_{int}}{\partial\dot{\psi}}(\tilde{\psi}, \tilde{\dot{\psi}}, \tilde{\ddot{\psi}}) &= C_t, \\
\frac{\partial F_{int}}{\partial\ddot{\psi}}(\tilde{\psi}, \tilde{\dot{\psi}}, \tilde{\ddot{\psi}}) &= M_t,
\end{aligned} \tag{21}$$

where K_t, C_t, and M_t denote the tangent stiffness, damping, and mass matrices. The tangent matrices are the derivatives of the internal force, but evaluated at the current Newton iteration. Substituting equations 20 and 21 into equation 16 yields

$$F_{int}(\psi, \dot{\psi}, \ddot{\psi}) = F_{int}(\tilde{\psi}, \tilde{\dot{\psi}}, \tilde{\ddot{\psi}}) + \left[K_t + \frac{\gamma}{\beta\Delta t}C_t + \frac{1}{\beta\Delta t^2}M_t\right]\Delta\psi. \tag{22}$$

Finally, substituting equation 22 into equation 11 yields

$$\left[K_t + \frac{\gamma}{\beta\Delta t}C_t + \frac{1}{\beta\Delta t^2}M_t\right]\Delta\psi = F_{ext} - F_{int}(\tilde{\psi}, \tilde{\dot{\psi}}, \tilde{\ddot{\psi}}) = Res. \tag{23}$$

Note that the right hand side of equation 23 is simply the residual, or the difference between the external force and the internal force at the current Newton iteration. As convergence occurs, the residual goes to

zero. As noted earlier, in the current implementation of the code we use the initial Newton method, which implies that $K_t = K$, $C_t = C$, and $M_t = M$, where K and M are defined in equation 3.

We now derive explicit expressions for K_t, C_t, and M_t. We have

$$\begin{aligned} K_t &= \frac{\partial F_{int}}{\partial \psi}(\tilde{\psi}, \tilde{\dot{\psi}}, \tilde{\ddot{\psi}}) \\ &= \int_\Omega \nabla N^T \cdot \nabla N d\Omega - \frac{2}{\rho c^2} \int_\Omega (\nabla \tilde{\dot{\psi}} \cdot \nabla N^T) N d\Omega, \end{aligned} \tag{24}$$

$$\begin{aligned} C_t &= \frac{\partial F_{int}}{\partial \dot{\psi}}(\tilde{\psi}, \tilde{\dot{\psi}}, \tilde{\ddot{\psi}}) \\ &= \frac{1}{c^2} \int_\Omega b \nabla N^T \cdot \nabla N d\Omega - \frac{2}{\rho c^2} \int_\Omega (\nabla \tilde{\psi} \cdot \nabla N^T) N d\Omega \qquad (25) \\ &- \frac{1}{\rho c^4} B/A \int_\Omega \tilde{\dot{\psi}} N^T N d\Omega, \qquad (26) \\ & \qquad (27) \end{aligned}$$

$$\begin{aligned} M_t &= \frac{\partial F_{int}}{\partial \ddot{\psi}}(\tilde{\psi}, \tilde{\dot{\psi}}, \tilde{\ddot{\psi}}) \\ &= \frac{1}{c^2} \int_\Omega N^T N d\Omega - \frac{1}{\rho c^2} B/A \int_\Omega \tilde{\dot{\psi}} N^T N d\Omega, \end{aligned} \tag{28}$$

where N is the vector of element shape functions.

The nonlinear formulation still contains the original stiffness and mass terms of the linear equation. However, the nonlinear formulation contains several additional terms. The stiffness portion of the nonlinear formulation now includes a reduction in the stiffness matrix noted by the second term in Eq. 24. This reduction is proportional to the particle velocity and the factor $\frac{2}{\rho c^2}$. The mass portion of the nonlinear formulation now includes a reduction in the mass matrix by the second term in Eq. 28. This reduction is proportional to the time derivative of the velocity potential and the factor $\frac{B}{A \rho c^2}$. Even though both the mass and the stiffness are being reduced, the stiffness terms are greater. This implies that energy in the lower frequencies will be driven to the higher frequencies. The nonlinear effects increase the frequency of the sound waves. In addition, the nonlinear formulation can handle waves with finite amplitude .

The nonlinear weak formulation, Eq. 10, still contains that same terms as the linear weak formulation, Eq. 2; however, there are several additional terms that would effect the matrices. Given the fact that now the internal force vector will depend on ψ and its first two time derivatives, a newton iteration is used to drive the residual to zero at the current time step. *The full implementation will be described in an appendix.*

For the full Newton method, these tangent matrices need to be reformed at each iteration of the Newton loop. The tangent damping and tangent stiffness matrices are *nonsymmetric*, since some terms involve products of shape functions with gradients of shape functions. However, we note that the *initial* tangent matrices are all symmetric, since at time $t = 0$, we have $\psi = 0$, $\dot{\psi} = 0$ and $\ddot{\psi} = 0$ by assumption. In that case, we have

$$K_{t_0} = \int_\Omega \nabla N^T \cdot \nabla N d\Omega, \tag{29}$$

$$C_{t_0} = \frac{1}{c^2} \int_\Omega b \nabla N^T \cdot \nabla N d\Omega, \tag{30}$$

$$M_{t_0} = \frac{1}{c^2} \int_\Omega N^T N d\Omega. \tag{31}$$

In this work we chose the Newton method for the nonlinear solution, and thus we could use any of the variants of this method, some requiring more and less frequent updating of the tangent matrices. In

the case of the full Newton method, the nonsymmetric tangent matrices would need to be reformed at each iteration. In the initial Newton method, only the initial symmetric tangent needs to be formed. The numerical experiments conducted thus far indicate that excellent convergence behavior is observed even with the initial Newton method.

In summary, the additional terms in the weak formulation, Eq. 10, affect the system by driving energy from lower frequencies to higher frequencies. The nonlinear effects increase the frequency of the sound waves. In addition, the nonlinear formulation can handle waves with finite amplitude.

III. When Do Acoustics Become Nonlinear?

Given the ability to simulate nonlinear acoustics, a simple method to determine if the acoustics are nonlinear would be to compare a linear acoustics simulation to a nonlinear simulation. This is done in Section IV. However, this is computationally costly. Even if the system is linear the nonlinear formulation will require at least two iterations per time step. Therefore, the following is derived as a guideline for when to use nonlinear acoustics.

Enflo and Hedberg state that nonlinear acoustics occurs when the Reynolds number is greater then or equal to one, $Re \geq 1$.[15] The Reynolds number can be defined for acoustics as[15]

$$Re = \frac{u\rho c}{b2\pi f}, \tag{32}$$

where u is particle velocity, ρ is density, c is phase speed, f is frequency and

$$b = \frac{(\gamma - 1)\kappa}{c_p} + \frac{4\eta}{3} + \zeta, \tag{33}$$

where γ is the ratio of specific heats (1.4), κ is the thermal conductivity, c_p is the specific heat at constant pressure, η is shear viscosity and ζ is bulk viscosity.

Using a plane wave approximation, $\frac{p}{u} = \rho c$, the Reynolds number can be written as

$$Re = \frac{p}{b2\pi f}. \tag{34}$$

However, in the nonlinear regime $\frac{p}{u}$ does not equal ρc, but at the edge of transition between linear and nonlinear it can be assumed to be correct. Equation 34 can be solved for the pressure given the constraint $Re \geq 1$ for the decibel ratio with a reference pressure, p_{ref}, of $2.0x10^{-5}\ Pa$.

$$dB = 20log_{10}\left(\frac{(Re)b2\pi f}{\sqrt{2}p_{ref}}\right). \tag{35}$$

This results in the transition to nonlinear acoustics as shown in Fig. 1.

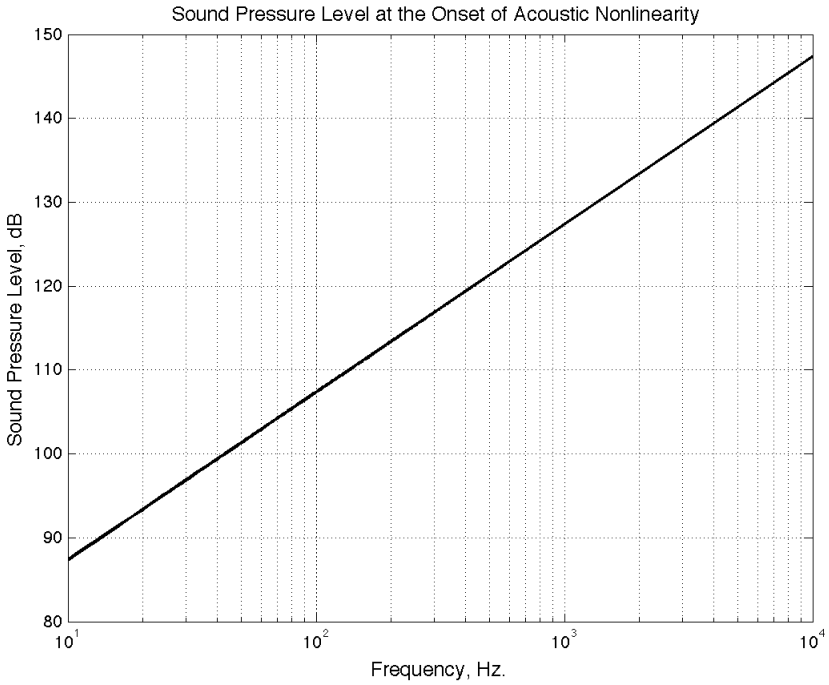

Figure 1. Relationship between linear and nonlinear acoustics as a function of acoustic frequency, where nonlinear acoustic are exhibited above the line.

IV. Comparisons to Acoustic Experiment

In order to provide confidence in the acoustic modeling capability of the SIERRA SD code and the analyst, an acoustic experiment was performed with a structural system that has been modeled. This section provides a brief description of the experiment, the simulation comparisons, and two methods to account for the nonlinear acoustic behavior.

IV.A. Experimental Description

Acoustic testing was recently performed on a store at Sandia National Laboratories in Albuquerque, NM. Using the scaled-down flight environment as a reference, overall sound pressure levels up to 130.5 dB were obtained in the reverberant chamber through the use of concert loud-speakers, a closed-loop control system, and control microphones. Additional response microphones placed in the chamber were used to characterize the acoustic field while accelerometers mounted to the test unit were used to measure the structural response of a store.

The desired OASPL of 148 dB was taken from MIL-STD-810E[16] for the center section of a store. This sound pressure level was not achievable in the current chamber due to amplifier limitations. Therefore, the overall specifications was scaled down to 130.5 dB OASPL. Eight tests were performed with two tests at each of the following OASPL levels: 121.5 dB, 124.5 dB, 127.5 dB, and 130.5 dB. The test were performed for 20 seconds each.

There were 17 microphones surrounding the store as depicted in Fig. 2. Eight of the microphones were used for control. The average control was well within ± 3 dB tolerance bands as shown in Fig. 3. There were also 70 accelerometers used with the majority on the exterior of the store as seen in Fig. 2. The microphone response is used to validate the input into the simulations, which is discussed in Section IV.B. The accelerometer responses are used for comparing the structural response, analyzed in Section IV.D. This assures proper coupling at the wetted interface as long as the structural model is valid.

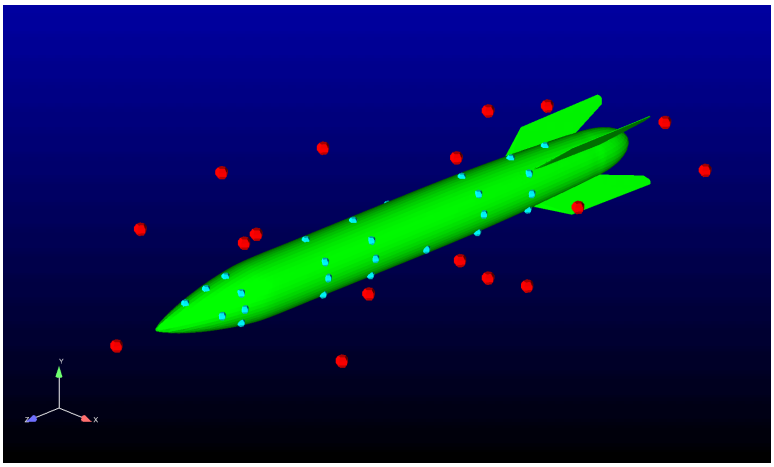

Figure 2. Microphone locations depicted in red and exterior accelerometer locations depicted in blue.

IV.B. Simulation Methodology

Finite Elements are used to model the system, where acoustic elements surround the store. This is notionally depicted in Fig. 4, where the blue cylinder structure is surrounded by green acoustic elements. A non-reflecting boundary (NRB) condition is applied to outer edge of the acoustic domain. There are two NRB conditions used in this work, the zero-th order approximation to the Sommerfeld condition and higher order infinite elements.

The input excitation is applied on the exterior of the acoustic domain where the NRB condition is implemented. An acoustic velocity is applied to patches on the outside domain. An example of patches is shown in Fig. 5. The input is inversely determined to match the specified diffuse field.

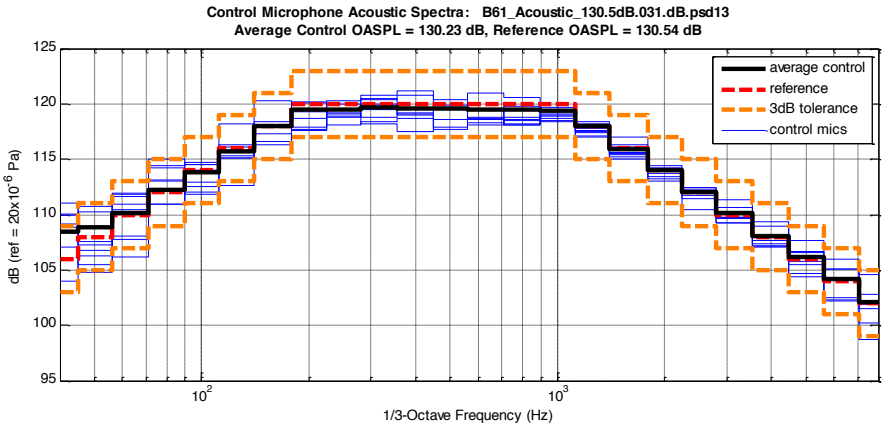

Figure 3. Control microphone performance for an acoustic test at 130.5 dB OASPL. The Average control is well within ± 3 dB.

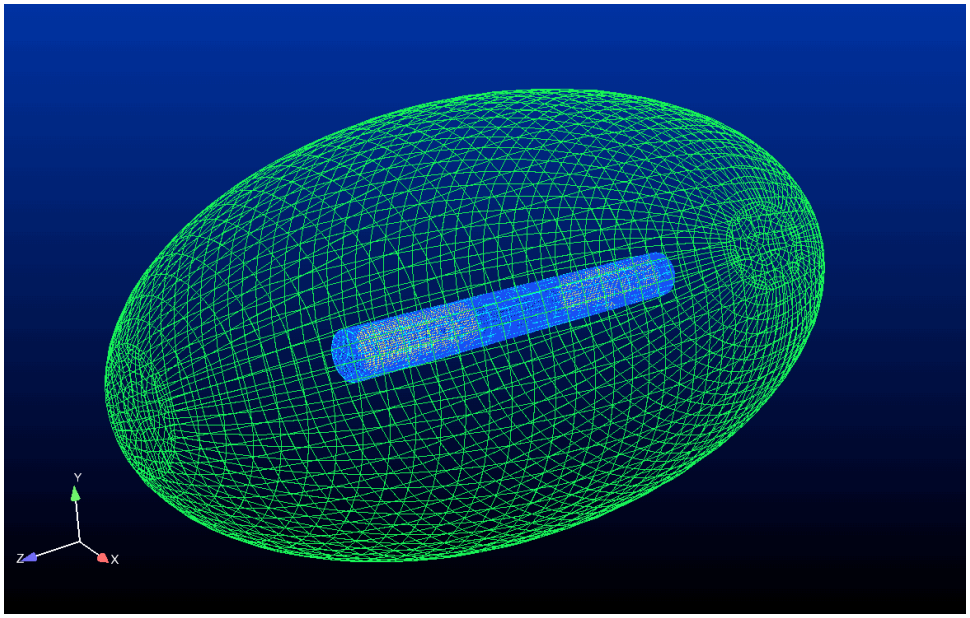

Figure 4. Finite element representation of a cylinder structure within an acoustic mesh.

IV.C. Building Confidence in Acoustic Modeling

In order to build confidence in the computational methodology as well as the analyst several studies were conducted: diffuse field no structure, diffuse field with structure, nonreflecting boundary study, and a dispersion study.

The first study was to determine if the acoustic mesh would provide a diffuse field with no structure inside the mesh. The mesh was scaled to $\frac{1}{10}th$ the original size. A 150 dB magnitude input was provided that ranged from 40 to 315 Hz. Each of the third octave frequency in the range is compared from the origin to the edge of the mesh. The results are shown in Fig. 6, where generally a diffuse field is shown.

A very similar study was conducted except a cylindrical structure was centered inside the acoustic mesh. The pressure was noted along the structural body. Figure 7 illustrates that in general the field is diffuse when a structure is present.

The nonreflecting boundary was studied by applying a pressure impulse at one end of the mesh and noting the pressure response at the center of the mesh. Figure 8 shows that there is no reflecting wave after the initial impulse passes the center. However, it does illustrate a concern with dispersion.

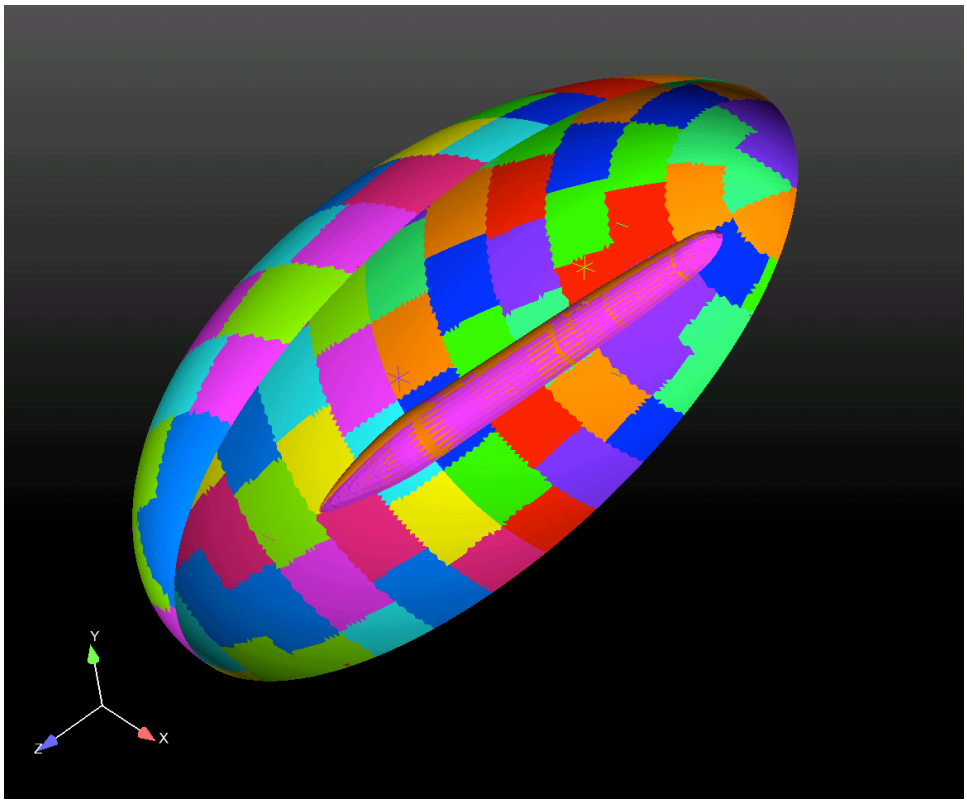

Figure 5. Patches on the outer edge of the acoustic domain used for applying the input.

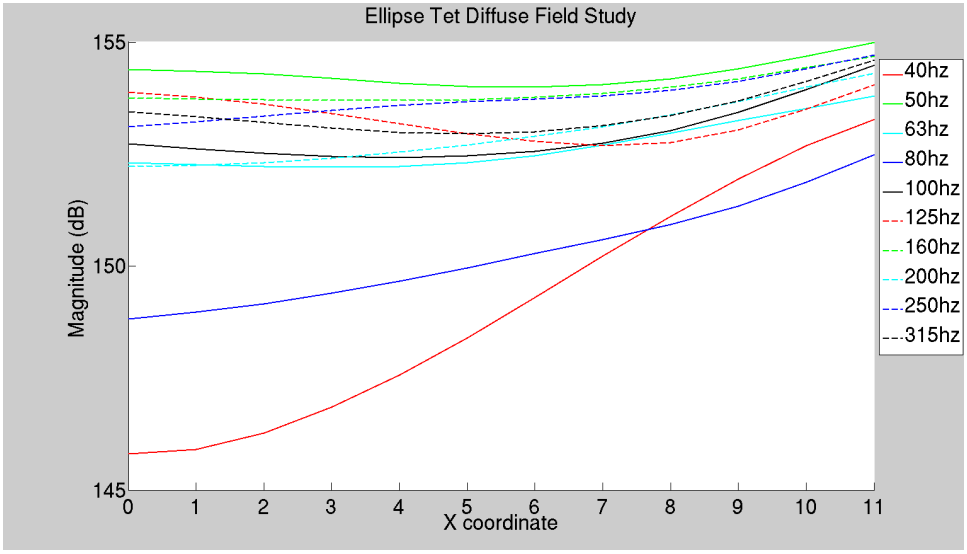

Figure 6. Diffuse field study where the X coordinate varies from the origin to the edge of the mesh.

A dispersion study was finally conducted. For this study, a cylindrical tube was created and a pressure wave impulse was applied at the left hand side. Figure 9 illustrates that there is some significant distortion to the pressure impulse.

The distortion is also noted in Fig. 10. The plane wave has obviously dispersed. Since the mesh is not sufficiently refined, the phase speed for the tetrahedral 4-node elements is higher than it should be causing

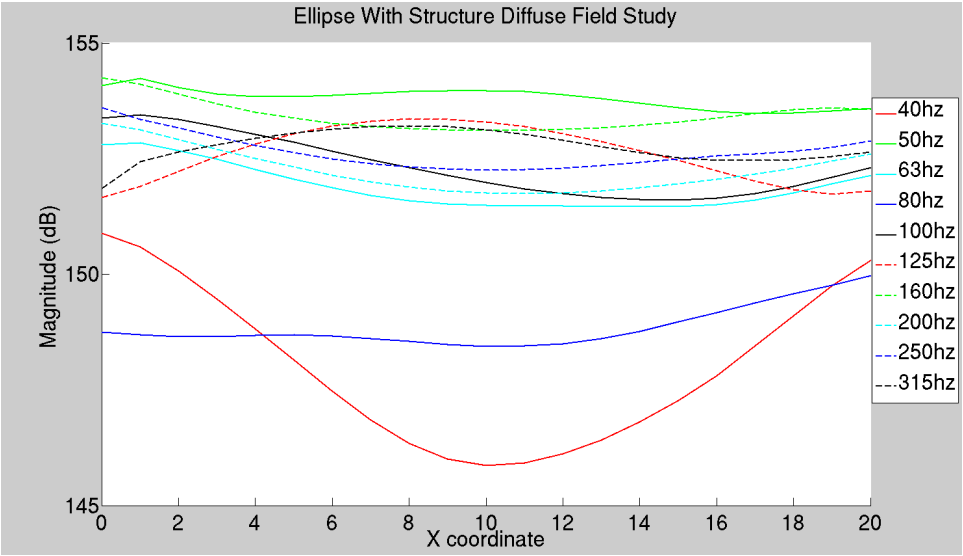

Figure 7. Diffuse field study including a cylindrical structure where the X coordinate varies from the left edge of the structure to the right edge of the structure.

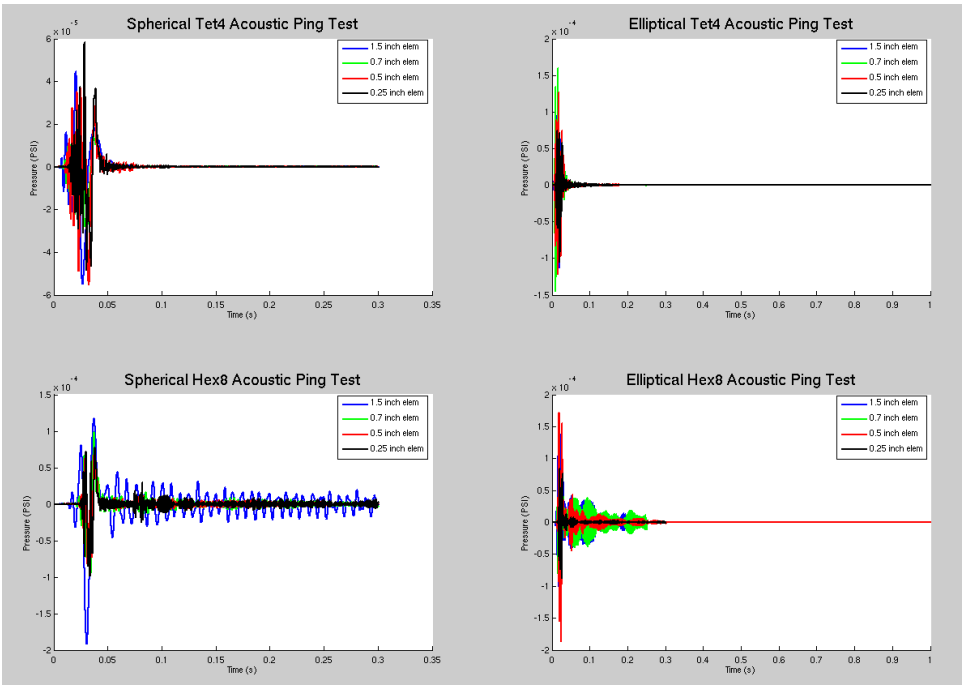

Figure 8. Demonstrating that the reflecting boundary is working by not seeing a reflective tone.

the plane wave to propagate faster than it should.

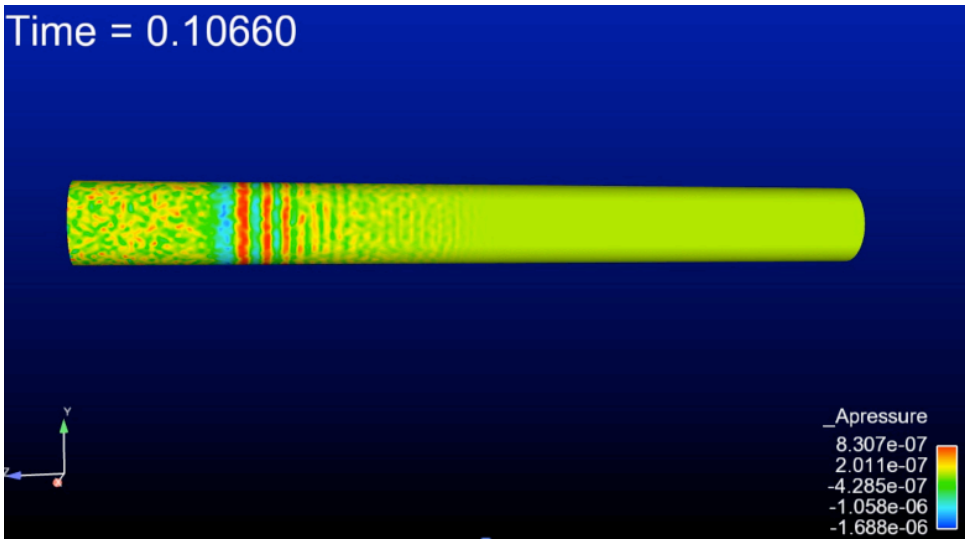

Figure 9. Dispersion test where a pressure wave impulse was applied to the left end of the acoustic cylindrical pressure tube.

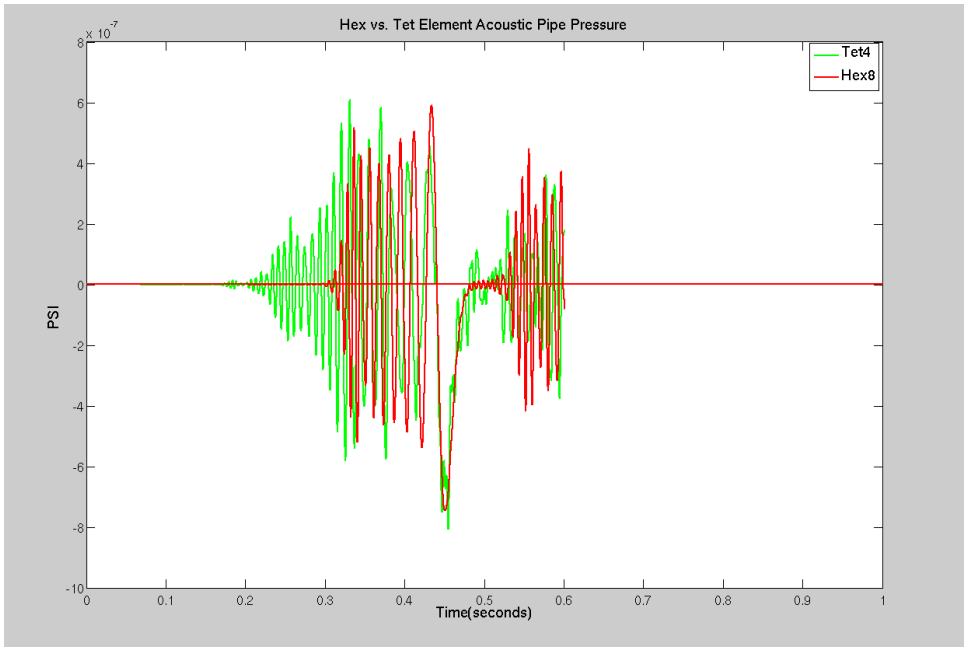

Figure 10. Dispersion test where a pressure wave impulse was applied to the left end of the acoustic cylindrical pressure tube.

IV.D. Simulation Comparisons to Experiment

According to Section III, the acoustic experiment is on the verge of exhibiting nonlinearity. Therefore, a linear and a nonlinear acoustic simulation is performed. Figure 11 shows the difference between the linear and nonlinear pressure response at one of the microphones. Though there is a subtle difference, it was decided that a linear analysis would be appropriate. To help confirm that the experiment acoustics was linear the microphone recorded pressures were compared to a normal distribution. It was found that the pressure generally followed a normal distribution, an example for one of the microphones is shown in Fig. 12.

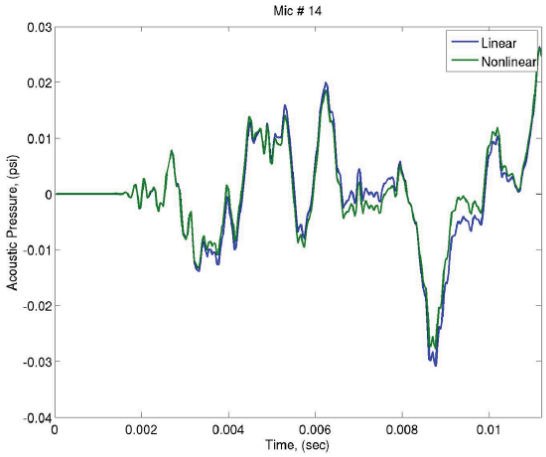

Figure 11. Linear versus nonlinear pressure response at one of the microphone locations.

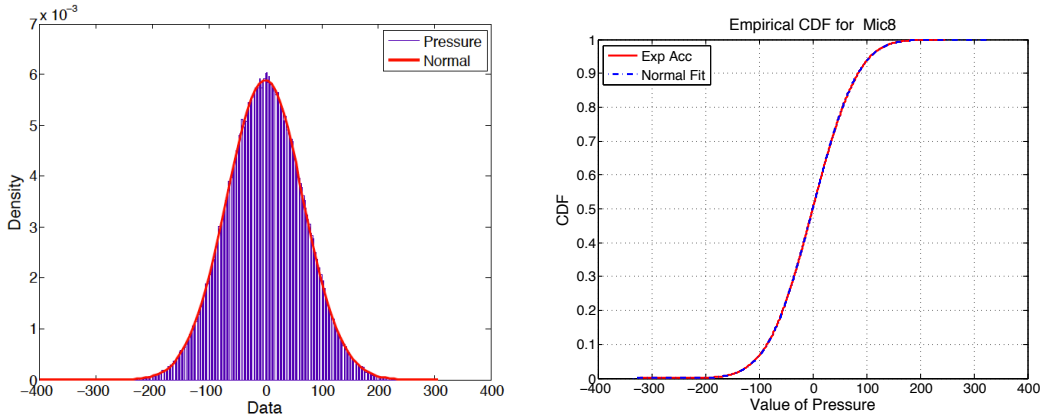

(a) PDF **(b)** CDF

Figure 12. Pressure distribution at microphone 8 demonstrating a normal distribution.

The second item checked in the simulation is if the average microphone response is the same as the microphone control response in the acoustic test. Figure 13 illustrates excellent agreement among the average responses. However, if individual microphones are examined, as in Fig. 14, one can see that the individual microphones do have some difference. However, none of the difference are greater then 7 dB in the frequencies of interest.

Finally, we compare acceleration responses between simulation and experiment for components of the structural system. Figure 15 shows the comparison between the simulation and the experiment. The error noticed is deemed acceptable for the simulations of interest.

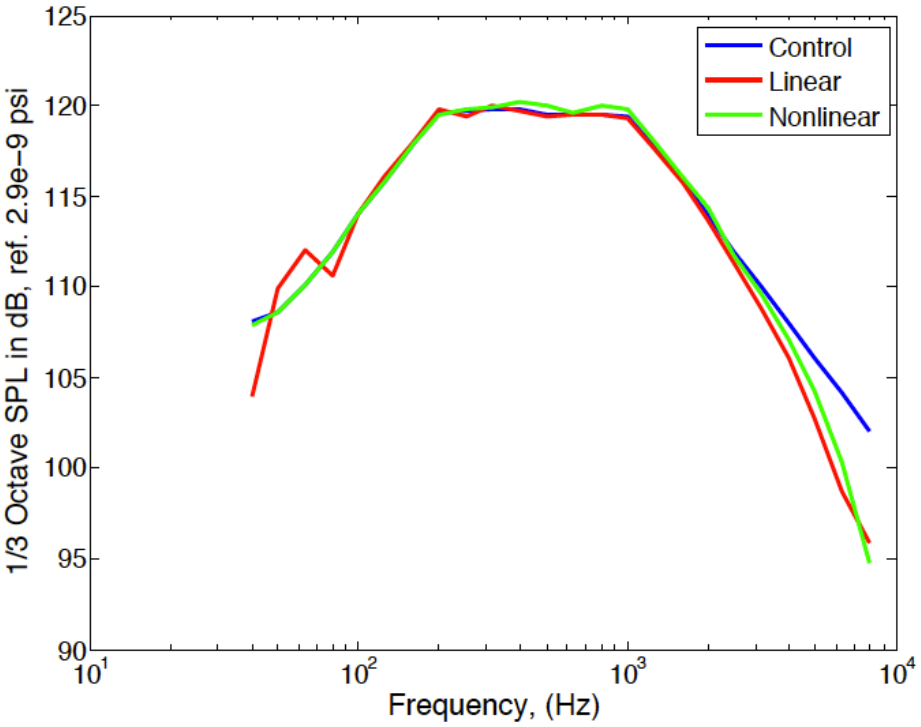

Figure 13. Simulation average microphone response compared to the control averages in the acoustic experiment.

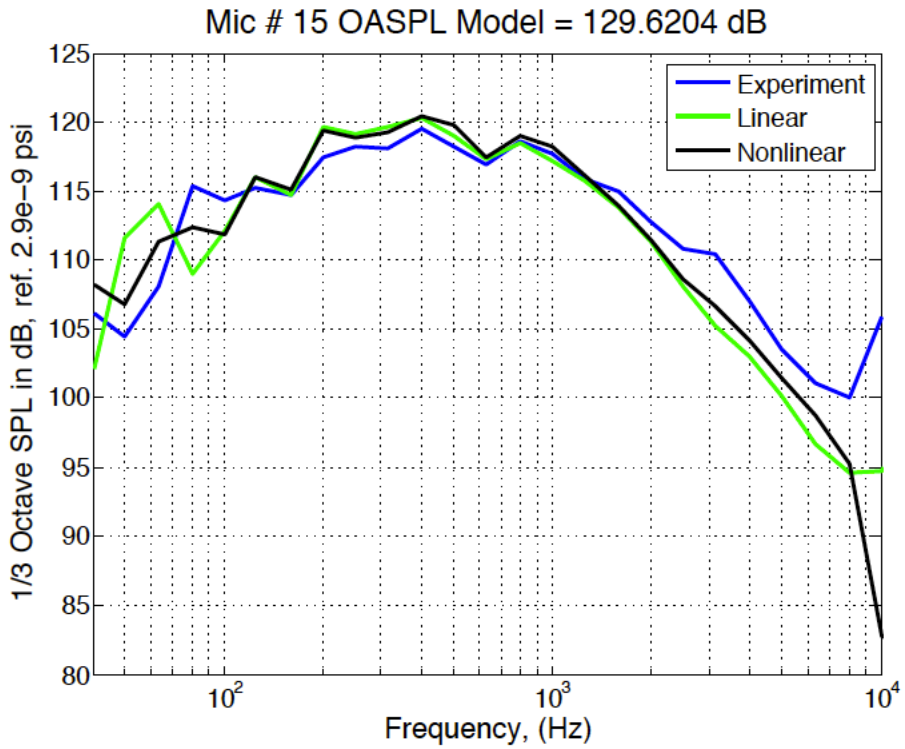

Figure 14. Microphone 15 pressure response comparing simulations to actual experiment.

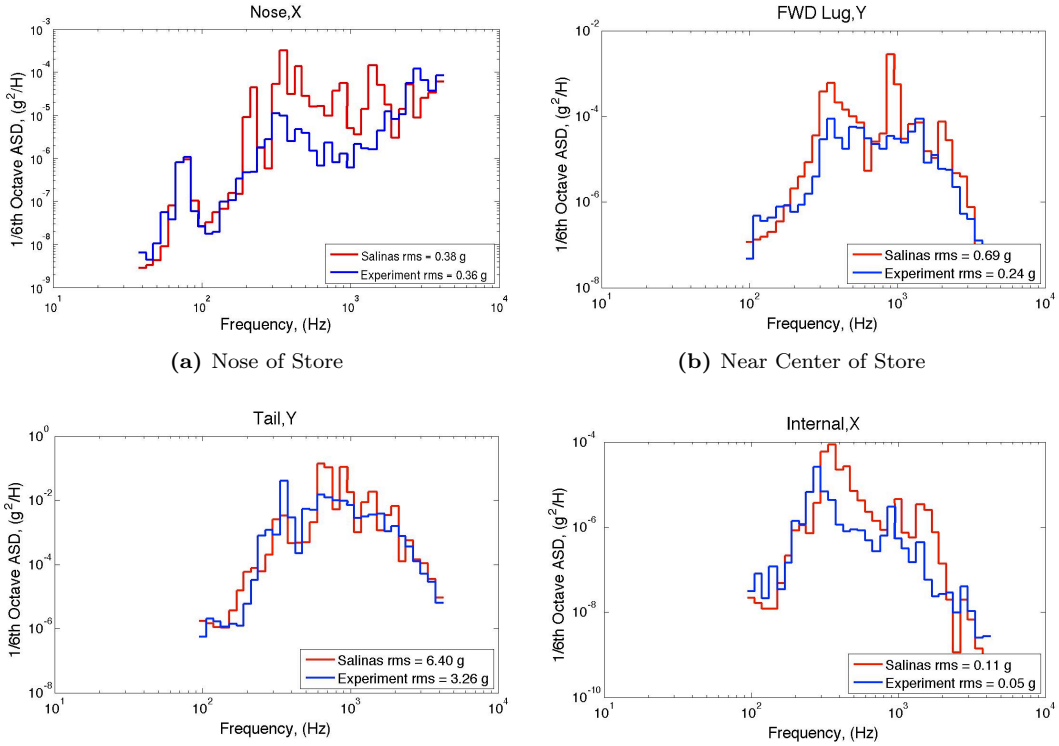

(a) Nose of Store

(b) Near Center of Store

(c) Tail of Store

(d) Internal Component

Figure 15. Acceleration response comparison between experiment and simulation at various locations.

V. Vibro-Acoustic Simulation Comparison to Flight Data

The ultimate goal is to be able to provide accurate environmental predictions at the component levels of the external captive carry store. Typically, the majority of the components inside the store are not instrumented. Before predictions at these components are believed accurate, comparisons are made between actual instrumented locations and simulations.

Sandia National Laboratories has collected a significant amount of flight data for one of their stores. The data was reviewed and the values reported here are for the same aircraft when it is flying at a constant velocity and level for a portion of time. Unfortunately, most flight profiles do not fly at the maximum dynamic pressure, Q, and the various flights are at different dynamic pressures. To overcome the varying dynamic pressures, a best fit linear line is established for each accelerometer. The best fit line is found by comparing the dynamic pressure to acceleration rms value for the particular period of time for the accelerometer. The slope of the best fit line is then used to scale the flight data set to max Q along the slope with the "Y" intercept being zero.

The acoustic input for the simulation was determined from the work by Cap et. al.,[4] except it was increased to an OASPL 155 dB. In Cap et. al. work, a "best effort" acoustic profile was found. The acoustic input is shown in Fig. 16.

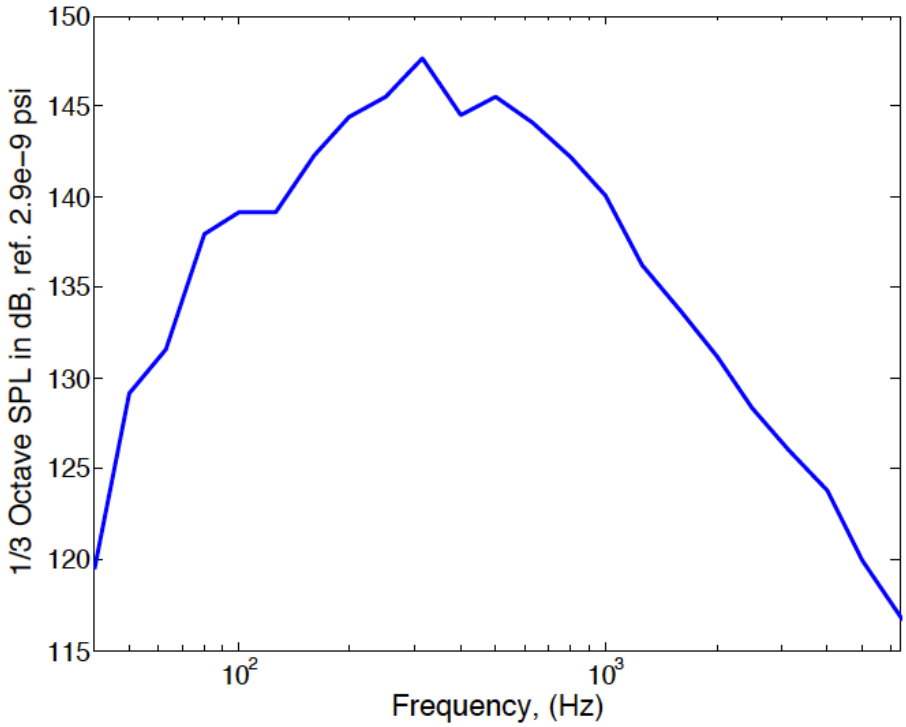

Figure 16. Acoustic profile input for simulations with an OASPL 155 dB.

There are two main physical phenomena that excite vibrations for stores of concern to Sandia National Laboratories. The first is the source due to aerodynamic flow over the store. Oscillating pressures within the flow drive vibration of the airframe surfaces.[17] This is accounted for with the acoustic simulation. The other main source of vibration in the store is the vibrations associated with carrying aircraft and are transmitted to the store through the attaching structure. This is simulated with a random vibration simulation. There are two input locations at the forward and aft lug in each of the Cartesian directions. The specifications for the inputs are based on the store environmental specifications and shown in Fig. 17. In the Fig. 17 the simulation input is compared to the desired input as a check for the simulation.

The attaching structure between the store and carrying aircraft are known to filter out high frequency excitation from the aircraft to the store. Therefore, only the random vibration responses below 200 Hz are superimposed with the acoustic response simulations for this work. In order to superimpose the two

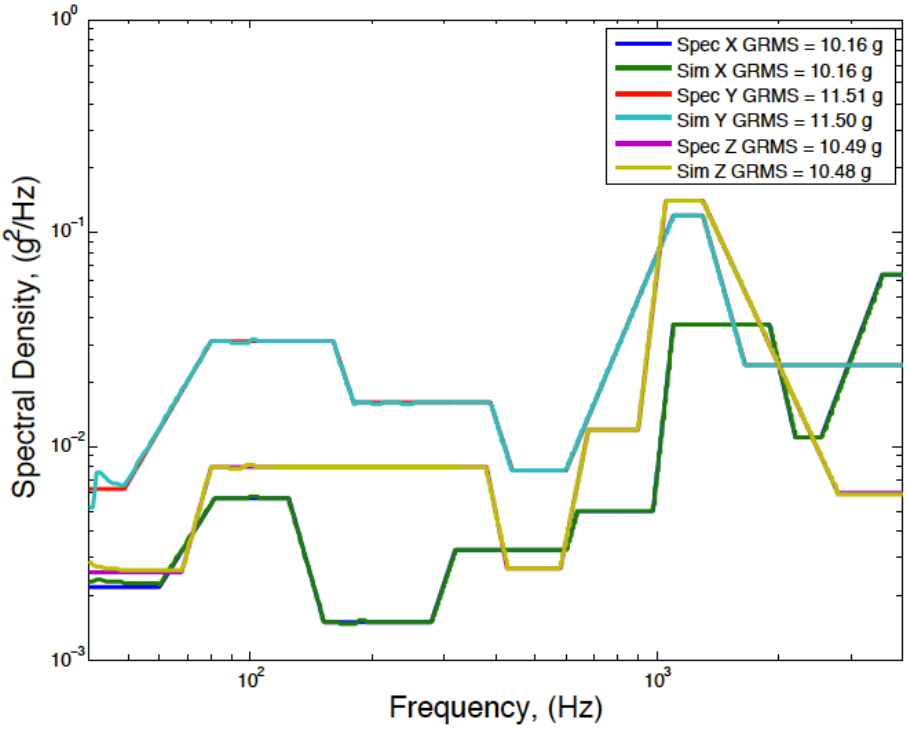

Figure 17. Random vibration input specification at the forward and aft lugs.

simulations, it is assumed that the response from the structural random vibration is uncorrelated to the response from acoustics.

A linear and a nonlinear acoustic simulation is performed with the new acoustic specification. Figure 18 shows the difference between the linear and nonlinear pressure response at one of the microphones. There is enough noticeable difference that a nonlinear acoustic run is required.

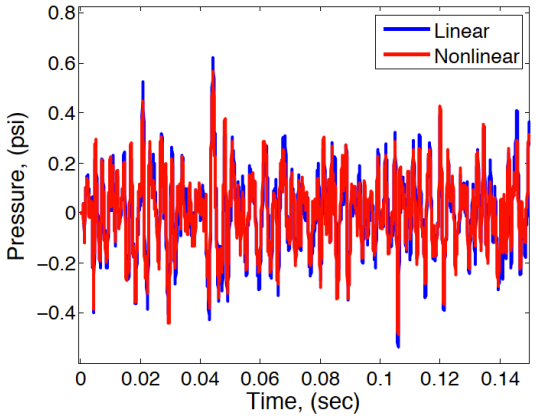

Figure 18. Linear versus nonlinear pressure response at location in the acoustic mesh.

A comparison for various locations between flight data and the simulations are shown in Fig. 19. The thick blue line represents the simulations. The thin lines represent the flight data. The flight data was provided in 1/6 Octave Auto-Spectral Density format. Therefore, the simulations were also provided in that format. As can be seen, the variation in the flight data is fairly large. Generally speaking, the simulations over predict or are within the variation of the flight data.

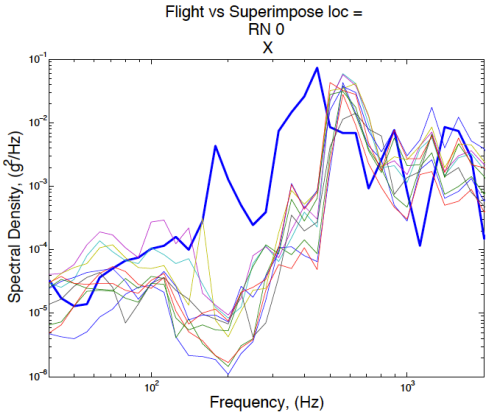

(a) Nose X-Dir.

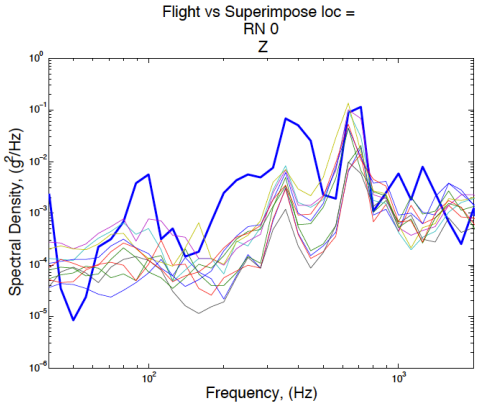

(b) Nose Z-Dir.

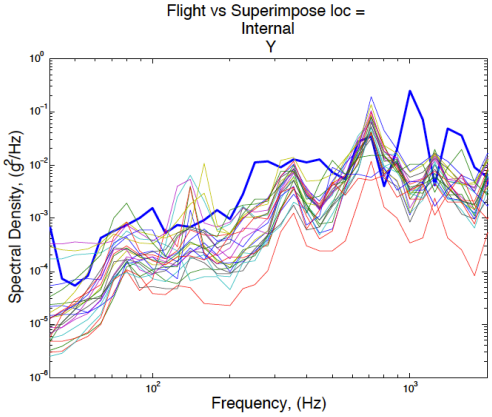

(c) Internal Component Y-Dir.

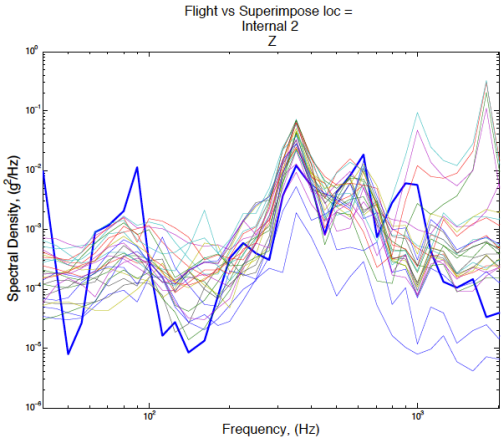

(d) Internal Component 2 Z-Dir.

Figure 19. Acceleration response comparison between flight data and simulation at various locations. The thick blue line represents the simulations. The thin lines represent the flight data.

VI. Conclusions

A nonlinear vibroacoustic method for simulating an external captive carried store acceleration response is presented in this work. The methodology for performing the simulation is verified by comparing to actual instrumented locations from flight tests. The model is calibrated with the use of a reverberant chamber acoustic experiment.

Future work in this area will continue with two main emphases. The first will be to provide a spatial varying load along the length of the store. This will allow for better inputs into the system by having different acoustic profiles along the length. The second emphasis will be on capturing the unsteady pressure loading beneath a turbulent boundary layer of a free store using statistical models which account for the magnitude, temporal, and spatial correlation of large coherent structures within the boundary layer.

Acknowledgments

Sandia National Laboratories is a multi-program laboratory managed and operated by Sandia Corporation, a wholly owned subsidiary of Lockheed Martin Corporation, for the U.S. Department of Energy's National Nuclear Security Administration under contract DE-AC04-94AL85000.

References

[1]Morton, M. H., Cox, J. T., and Powell, E. A., "Initial Assessment of a CFD Application for Predicting Jet Fighter Aircraft Cavity Bay Acoustics for Subsonic and Supersonic Aircraft States," 53rd AIAA Structures, Structural Dynamics, and Materials Conference, AIAA, Hawaii, April.

[2]Johnson, R., Kannepalli, C., Arunajatesan, S., and Sinha, N., "Computational Modeling of Geometrically-Complex Weapons Bays," *HPCMP Users Group Conference*, Vol. 0, 2010, pp. 77–82.

[3]DeChant, L. and Payne, J., "A Convection Reaction Diffusion (CRD) Equation Model for 2-d Transition Pressure Fluctuation Behavior," *AIAA Paper 2008-3020*, May 2008.

[4]Cap, J. S., Togami, T. C., and Hollingshead, J. R., "A Comparison of the Response of a Captive Carried Store to Both Reverberant and Progressive Wave Acoustic Excitation and the Field Environment," Tech. Rep. SAND96-1410C, Sandia National Labs, September 1996.

[5]Reese, G., Bhardwaj, M., and Walsh, T., "Salinas- Theory Manual," Tech. Rep. SAND2009-0748, Sandia National Labs, Albuquerque, NM, 2009.

[6]Chung, Y. T., Krebs, D. J., Tong, H., and Fulcher, C. W. G., "Validation of Component Vibrations Predicted from Response Matching Method By Finite Element Acoustic Analysis," 53rd AIAA Structures, Structural Dynamics, and Materials Conference, AIAA, Hawaii, April.

[7]Gloyna, F. L., "Vibroacoustic Response Using the Finite Element Method and Statistical Energy Analysis," 59th Shock and Vibration Symposium, Albuquerque, NM, October 1988.

[8]Walsh, T. and Torres, M., "Finite Element Methods for Nonlinear Acoustics in Fluids," *Journal of Computational Acoustics*, Vol. 15, No. 3, 2007, pp. 353–375.

[9]Allen, H. W., "Modeling Realistic Environmental Stresses on External Stores," *Journal of Environmental Sciences*, September/October 1985.

[10]Poyner, S. P., "Air-to-Air Missile Airframe Captive Flight Vibro-Acoustic Environment," *Journal of IES*, July/August 1990.

[11]Hamilton, M. F. and D. T. Blackstock, E., *Nonlinear Acoustics*, Academic Press, 1998.

[12]Beyer, R. T., *Nonlinear Acoustics*, Department of the Navy, Sea Systems Command, 1974.

[13]Naugolnykh, K. and Ostrovsky, L., *Nonlinear Wave Processes in Acoustics*, Cambridge University Press, 1998.

[14]Kuznetsov, V. P., "Equations of Nonlinear Acoustics," *Sov. Phys. Acoust.*, Vol. 16, 1971, pp. 467–470.

[15]Enflo, B. O. and Hedberg, C. M., *Theory of Nonlinear Acoustics in Fluids*, Kluwer Academic Publishers, 2002.

[16]MIL-STD-810E, *Environmental Test Methods and Engineering Guidelines*, Department of Defense.

[17]MIL-STD-810G, *Environmental Engineering Considerations and Laboratory Tests*, Department of Defense, Oct 2008.